

A weak lensing view on primordial non-Gaussianities

Björn Malte Schäfer^{1*}, Alessandra Grassi¹, Mischa Gerstenlauer² and Christian T. Byrnes³

¹*Astronomisches Recheninstitut, Zentrum für Astronomie, Universität Heidelberg, Mönchhofstraße 12, 69120 Heidelberg, Germany*

²*Institut für theoretische Physik, Universität Heidelberg, Philosophenweg 16, 69120 Heidelberg, Germany*

³*Fakultät für Physik, Universität Bielefeld, Postfach 100131, 33501 Bielefeld, Germany*

11 July 2011

ABSTRACT

We investigate the signature of primordial non-Gaussianities in the weak lensing bispectrum, in particular the signals generated by local, orthogonal and equilateral non-Gaussianities. The questions we address include the signal-to-noise ratio generated in the Euclid weak lensing survey (we find the 1σ -errors for f_{NL} are 200, 575 and 1628 for local, orthogonal and equilateral non-Gaussianities, respectively), misestimations of f_{NL} if one chooses the wrong non-Gaussianity model (misestimations by up to a factor of ± 3 in f_{NL} are possible, depending on the choice of the model), the probability of noticing such a mistake (improbably large values for the χ^2 -functional occur from $f_{\text{NL}} \sim 200$ on), degeneracies of the primordial bispectrum with other cosmological parameters (only the matter density Ω_m plays a significant role), and the subtraction of the much larger, structure-formation generated bispectrum. If a prior on a standard Λ CDM-parameter set is available from Euclid and Planck, the structure formation bispectrum can be predicted accurately enough for subtraction, and any residual structure formation bispectrum would influence the estimation of f_{NL} to a minor degree. Configuration-space integrations which appear in the evaluation of χ^2 -functionals and related quantities can be carried out very efficiently with Monte-Carlo techniques, which reduce the complexity by a factor of $\mathcal{O}(10^4)$ while delivering sub-percent accuracies. Weak lensing probes smaller scales than the CMB and hence provide an additional constraint on non-Gaussianities, even though they are not as sensitive to primordial non-Gaussianities as the CMB.

Key words: cosmology: large-scale structure, gravitational lensing, methods: analytical

1 INTRODUCTION

As cosmological data improves, it is becoming increasingly feasible to probe models of the early universe. In particular, primordial non-Gaussianity has emerged as a leading window onto the physics of inflation and the early universe (for reviews, see Bartolo et al. 2004; Komatsu 2010; Langlois 2011). Although non-Gaussian perturbations could in principle take any form, in practice searching for just a few shapes of the bispectrum (3-point correlation function) allows one to discriminate between entire classes of models (Bernardeau & Uzan 2003; Komatsu et al. 2009; Komatsu et al. 2011). Many alternative models to inflation produce the same non-Gaussian shapes, and therefore can also be constrained at the same time.

The theory of primordial non-Gaussianities is very evolved, and predictions for non-Gaussianities in different observational channels have been made: number counts and large-scale structure statistics (Verde 2010; Desjacques & Seljak 2010a,b; Fedeli et al. 2011), the cosmic microwave background even outside the Sachs-Wolfe regime (Fergusson & Shellard 2007; Fergusson et al. 2010)

and gravitational lensing (Fedeli et al. 2011; Pace et al. 2011; Marian et al. 2011; Jeong et al. 2011).

Most constraints on non-Gaussianities are reported using CMB-observations, either by measuring the bispectrum of the temperature perturbation directly (Komatsu 2003; Creminelli et al. 2006; Yadav & Wandelt 2008; Curto et al. 2009; Komatsu et al. 2009; Vielva & Sanz 2009, 2010; Casaponsa et al. 2011), by measuring the skewness of weighted averaged CMB-patches (Mukherjee & Wang 2004) or by quantifying the corresponding Minkowski functionals (Cabella et al. 2005; Gott et al. 2007; Hikage et al. 2008). The tightest bounds on the amplitude f_{NL} of the bispectrum, $-10 \leq f_{\text{NL}} \leq 74$ has been obtained by Komatsu et al. (2011).

So far, observational constraints on the weak lensing bispectrum (Bernardeau et al. 2003; Shi et al. 2011) mainly concerned the non-Gaussianities generated by structure formation and their breaking of the Ω_m - σ_8 degeneracy (Ménard et al. 2003), and first results have been obtained using the skewness of the aperture-mass statistic (Schneider et al. 1998; Semboloni et al. 2011).

In this paper we forecast the constraints which the weak lensing bispectrum will be able to make on primordial non-Gaussianity, especially with a view to Euclid. Although the constraints are not competitive with the CMB if the non-Gaussianities are scale inde-

* e-mail: bjoern.malte.schaefer@uni-heidelberg.de

pendent, they are complementary since they probe smaller scales compared to the CMB and provide constraints on a possible scale-dependence (Lo Verde et al. 2008). A scale dependence of f_{NL} at the same order as the spectral index of the power spectrum is natural (Byrnes et al. 2010) and it may be much stronger, e.g. a “step-function” which is zero on large scales and large on small scales (Riotto & Sloth 2011). Weak lensing also has lower systematic errors than other large scale structure probes such as the galaxy bispectrum, scale dependent bias and cluster counts. Because the weak shear provides a linear mapping of the cosmic matter distribution, the statistical properties of the source field are conserved in the observable.

After a brief recapitulation of cosmology and structure formation in Sect. 2 we introduce primordial and structure formation non-Gaussianities in Sect. 3, in particular the bispectral shapes and the motivation for studying them. The mapping of non-Gaussianities by weak gravitational lensing is treated in Sect. 4, where we investigate the properties of the weak lensing bispectrum in its scale- and configuration dependence, and how it builds up as a function of survey depth. Statistical questions concerning the signal strength and misestimations of the non-Gaussianity parameter are addressed in Sect. 5, before we focus on systematic errors in the non-Gaussianity parameter due to incompletely removed structure formation non-Gaussianities in Sect. 6. We summarise our main results in Sect. 7 and provide visualisations of the weak lensing bispectrum sourced by different non-Gaussianity shapes in Appendix A.

The reference cosmological model used is a spatially flat w CDM cosmology with Gaussian adiabatic initial perturbations for the cold dark matter density. The specific parameter choices are $\Omega_m = 0.25$, $n_s = 1$, $\sigma_8 = 0.8$, $\Omega_b = 0.04$ and $H_0 = 100h \text{ km/s/Mpc}$, with $h = 0.72$. The dark energy equation of state is constant in time with a value of $w = -0.9$.

2 COSMOLOGY AND STRUCTURE FORMATION

In spatially flat dark energy cosmologies with the matter density parameter Ω_m , the Hubble function $H(a) = d \ln a / dt$ is given by

$$\frac{H^2(a)}{H_0^2} = \frac{\Omega_m}{a^3} + \frac{1 - \Omega_m}{a^{3(1+w)}}, \quad (1)$$

for a constant dark energy equation of state-parameter w . Comoving distance χ and scale factor a are related by

$$\chi = c \int_a^1 \frac{da}{a^2 H(a)}, \quad (2)$$

such that the comoving distance is given in units of the Hubble distance $\chi_H = c/H_0$. For the linear matter power spectrum $P(k)$ which describes the Gaussian fluctuation properties of the linearly evolving density field δ ,

$$\langle \delta(\mathbf{k}) \delta(\mathbf{k}') \rangle = (2\pi)^3 \delta_D(\mathbf{k} + \mathbf{k}') P(k) \quad (3)$$

the ansatz $P(k) \propto k^{n_s} T^2(k)$ is chosen with the transfer function $T(k)$, which is well approximated by the fitting formula

$$T(q) = \frac{\ln(1 + 2.34q)}{2.34q} \times p(q)^{-1/4}, \quad (4)$$

for low-matter density cosmologies (Bardeen et al. 1986). The polynomial $p(q)$ is given by $p(q) = 1 + 3.89q + (16.1q)^2 + (5.46q)^3 + (6.71q)^4$. The wave vector $k = q\Gamma$ enters rescaled by the shape parameter Γ (Sugiyama 1995),

$$\Gamma = \Omega_m h \exp \left[-\Omega_b \left(1 + \frac{\sqrt{2h}}{\Omega_m} \right) \right]. \quad (5)$$

The fluctuation amplitude is normalised to the value σ_8 on the scale $R = 8 \text{ Mpc}/h$,

$$\sigma_R^2 = \frac{1}{2\pi^2} \int dk k^2 W_R^2(k) P(k), \quad (6)$$

with a Fourier-transformed spherical top-hat $W_R(k) = 3 j_1(kR)/(kR)$ as the filter function. $j_\ell(x)$ denotes the spherical Bessel function of the first kind of order ℓ (Abramowitz & Stegun 1972). The linear growth of the density field, $\delta(\mathbf{x}, a) = D_+(a)\delta(\mathbf{x}, a=1)$, is described by the growth function $D_+(a)$, which is the solution to the growth equation (Turner & White 1997; Wang & Steinhardt 1998; Linder & Jenkins 2003),

$$\frac{d^2}{da^2} D_+(a) + \frac{1}{a} \left(3 + \frac{d \ln H}{d \ln a} \right) \frac{d}{da} D_+(a) = \frac{3}{2a^2} \Omega_m(a) D_+(a). \quad (7)$$

3 NON-GAUSSIANITIES

3.1 Primordial non-Gaussianities

We write the primordial bispectra in terms of the Bardeen curvature perturbation Φ (Bardeen 1980; Bardeen et al. 1983), which may be related to the primordial curvature perturbation $\zeta = 5\Phi/3$ (see e.g. chapter 8 in Riotto 2002) and the CMB temperature anisotropy in the Sachs-Wolfe limit $\Delta T/T = -\Phi/3$ (Sachs & Wolfe 1967). The bispectrum of Φ is defined by

$$\langle \Phi(\mathbf{k}_1) \Phi(\mathbf{k}_2) \Phi(\mathbf{k}_3) \rangle = (2\pi)^3 \delta_D(\mathbf{k}_1 + \mathbf{k}_2 + \mathbf{k}_3) B_\Phi(k_1, k_2, k_3). \quad (8)$$

We will be particularly interested in three bispectral shapes, which cover the expected shape from a wide range of inflationary models (Komatsu 2010). They are defined as:

(i) **Local shape.** This is defined by

$$B_\Phi^{\text{local}}(k_1, k_2, k_3) = 2A^2 f_{\text{NL}}^{\text{local}} \left(k_1^{n_s-4} k_2^{n_s-4} + (2 \text{ perm}) \right), \quad (9)$$

where the amplitude A is defined by $P_\Phi(k) = Ak^{n_s-1}$. It may arise through a simple Taylor expansion about the Gaussian (linearised) perturbation $\Phi(x) = \Phi_G(x) + f_{\text{NL}} \Phi_G^2$, although this is not the most general ansatz for Φ which gives rise to the local bispectrum. The local shape typically arises from super-horizon evolution of the curvature perturbation ($k \ll aH$), which occurs for example in some multifield inflation models (Byrnes et al. 2008; Elliston et al. 2011), during modulated reheating (Dvali et al. 2004), in the curvaton scenario (Lyth et al. 2003) (the last three models are closely connected (Alabidi et al. 2010)), as well as the ekpyrotic scenario (Lehners 2010) and non-local inflation (Barnaby & Cline 2008).

(ii) **The equilateral shape** is given by

$$B_\Phi^{\text{equil}}(k_1, k_2, k_3) = 6A^2 f_{\text{NL}}^{\text{equil}} \left(-2(k_1 k_2 k_3)^{2(n_s-4)/3} - [(k_1 k_2)^{(n_s-4)} + (2 \text{ perm})] + [k_1^{(n_s-4)/3} k_2^{2(n_s-4)/3} k_3^{n_s-4} + (5 \text{ perm})] \right). \quad (10)$$

This shape typically arises in models with non-canonical kinetic terms, the most studied example being Dirac-Born-Infeld inflation (Silverstein & Tong 2004; Alishahiha et al. 2004). Also various other models can produce this shape (Arkani-Hamed et al. 2004; Seery & Lidsey 2005; Chen et al. 2007; Cheung et al. 2008; Li et al. 2008).

(iii) The **orthogonal shape** is given by

$$B_{\Phi}^{\text{ortho}}(k_1, k_2, k_3) = 6A^2 \int_{\text{NL}}^{\text{ortho}} \left(-8(k_1 k_2 k_3)^{2(n_s-4)/3} - 3 \left[(k_1 k_2)^{(n_s-4)} + (2 \text{ perm}) \right] + 3 \left[k_1^{(n_s-4)/3} k_2^{2(n_s-4)/3} k_3^{n_s-4} + (5 \text{ perm}) \right] \right), \quad (11)$$

(Senatore et al. 2010) and it was constructed in order to be orthogonal to both the equilateral shape and to a lesser extent the local shape.

The local model is maximised for squeezed triangles $k_1 \ll k_2 \simeq k_3$, the equilateral model is maximised for equilateral triangles $k_1 \simeq k_2 \simeq k_3$ while the orthogonal model receives contributions from a broader range of triangles. Another frequently considered shape is the enfolded one, which is maximised for “flattened” isosceles triangles $k_1 \simeq k_2 \simeq k_3/2$, but this can be written as a linear combination of the three shapes above. We note that although the above three shapes cover many classes of non-Gaussian models, there do exist other shapes which cannot be written as a combination of the above three shapes including localised or oscillating bispectra, which may be caused by a feature in the inflatons potential (Chen et al. 2007; Arroja et al. 2011), particle production while observable modes are crossing the horizon (Barnaby 2010) (but a burst of particle production later in inflation generates local non-Gaussianity, Battfeld et al. 2011), or an inflaton potential with superimposed oscillations (Chen et al. 2008; Chen 2011).

Because f_{NL} for all three shapes is normalised to an equilateral triangle, but the signal-to-noise is maximised for different triangle shapes depending on the configuration it is not surprising that the error bars on the three shapes are significantly different (Fergusson & Shellard 2009). In line with this expectation, we find that weak lensing can constrain the local model most tightly and the equilateral model least well. When investigating relative magnitudes between structure formation bispectra and primordial ones, we restrict ourselves to the equilateral case, as all primordial bispectra have equal values for this configuration. An alternative normalisation was proposed by Fergusson & Shellard (2009).

A mild scale dependence of f_{NL} is natural, for both the local model (Byrnes et al. 2010; Byrnes et al. 2010; Huang 2010), and the equilateral and orthogonal models (Chen 2005; Bartolo et al. 2010; Noller & Magueijo 2011; Burrage et al. 2011), and it may be much stronger, e.g. a “step-function” which is zero on large scales and large on small scales (Riotto & Sloth 2011). Although we treat f_{NL} as constant in this paper, the motivation for considering scale-dependence is important because weak lensing probes smaller scales than the CMB and hence the CMB bounds may not apply here, see Sec. 4. Observational probes have been considered in (Lo Verde et al. 2008; Sefusatti et al. 2009; Shandera et al. 2011; Becker et al. 2011).

For converting the bispectrum of the potential fluctuations to those of the density field we use the Newtonian Poisson equation for each occurrence of the potential in the bispectrum (Munshi et al. 2011),

$$\Delta \Phi = \frac{3}{2} \frac{\Omega_m}{\chi_H^2} \delta \rightarrow \delta(k, a) = \frac{2}{3\Omega_m} D_+(a) (\chi_H k)^2 T(k) \Phi(k) \quad (12)$$

The horizon entry of each mode is governed by the transfer function $T(k)$ and it grows $\propto D_+(a)$ in the linear regime, such that

$$B_{\delta}(k_1, k_2, k_3, a) = \prod_{i=1}^3 \left(\frac{2}{3\Omega_m} D_+(a) (\chi_H k_i)^2 T(k_i) \right) B_{\Phi}(k_1, k_2, k_3). \quad (13)$$

We choose the normalisation factor A to be consistent for each linearly evolving mode of the density field with our definition of σ_8 .

3.2 Non-Gaussianities from structure formation

Nonlinear processes in structure formation break the homogeneity of the growth equation and generate non-Gaussian features in the initially close to Gaussian density field. From Eulerian perturbation theory (see Sahni & Coles 1995; Bernardeau et al. 2002; Matsubara 2011; Scoccimarro & Couchman 2001), the first order contribution to the bispectrum $B_{\delta}(\mathbf{k}_1, \mathbf{k}_2, \mathbf{k}_3)$ (for an introduction, see Fry 1984a,b) of the density field from nonlinear structure formation is given by:

$$B_{\delta}(\mathbf{k}_1, \mathbf{k}_2, \mathbf{k}_3, a) = \sum_{\substack{i,j=1,2,3 \\ i \neq j}} D_+^4(a) M(\mathbf{k}_i, \mathbf{k}_j) P(k_i) P(k_j), \quad (14)$$

where the classical mode coupling function is $M(\mathbf{k}_i, \mathbf{k}_j)$

$$M(\mathbf{k}_i, \mathbf{k}_j) = \frac{10}{7} + \left(\frac{k_i}{k_j} + \frac{k_j}{k_i} \right) x + \frac{4}{7} x^2. \quad (15)$$

$x = \mathbf{k}_i \cdot \mathbf{k}_j / (k_i k_j)$ denotes the cosine between the wave vectors \mathbf{k}_i and \mathbf{k}_j . Due to the fact that $P(k, a)$ grows $\propto D_+^2(a)$ in linear structure formation, the bispectrum scales with $D_+^4(a)$ in lowest order perturbation theory. In terms of non-Gaussianity parameters and configuration dependences, structure formation non-Gaussianities are strongest for the squeezed configuration because the mode coupling function $M(\mathbf{k}_i, \mathbf{k}_j)$ assumes the largest values for parallel wave vectors (with the cosine being one, $x = 1$), and therefore resembles non-Gaussianities of the local type. Their strength in the weak shear bispectrum corresponds to an f_{NL} -parameter of $\mathcal{O}(10^4)$, i.e. two orders of magnitude larger than the primordial non-Gaussianities weak lensing can probe.

4 WEAK GRAVITATIONAL LENSING

4.1 Convergence spectrum

The weak lensing convergence κ follows from a line-of-sight integration weighted with the lensing efficiency $W_{\kappa}(\chi)$ (for reviews, see Bartelmann & Schneider 2001; Bartelmann 2010),

$$\kappa = \int_0^{\chi_H} d\chi W_{\kappa}(\chi) \delta \quad (16)$$

and reflects, because of its linearity, all statistical properties of the density field δ . The weak lensing efficiency is given by

$$W_{\kappa}(\chi) = \frac{3\Omega_m}{2a} \frac{1}{\chi_H^2} G(\chi) \chi, \quad (17)$$

with the weighted distance distribution $G(\chi)$ of the lensed galaxies,

$$G(\chi) = \int_{\chi}^{\chi_H} d\chi' q(z) \frac{dz}{d\chi'} \frac{\chi' - \chi}{\chi'}. \quad (18)$$

The spectrum $C_{\kappa}(\ell)$ then results from applying Limber’s equation (Limber 1954),

$$C_{\kappa}(\ell) = \int_0^{\chi_H} \frac{d\chi}{\chi^2} W_{\kappa}^2(\chi) P(k = \ell/\chi, a). \quad (19)$$

For the galaxy redshift distribution $q(z)$ we assume a standard shape,

$$q(z) = q_0 \left(\frac{z}{z_0} \right)^2 \exp \left(- \left(\frac{z}{z_0} \right)^{\beta} \right) dz \quad \text{with} \quad \frac{1}{q_0} = \frac{z_0}{\beta} \Gamma \left(\frac{3}{\beta} \right), \quad (20)$$

with the median redshift set to 0.9, as projected for Euclid.

4.2 Convergence bispectrum

Similarly as in the case of the weak shear spectrum $C_\kappa(\ell)$ we use the Limber-equation in the flat-sky approximation,

$$B_\kappa(\ell_1, \ell_2, \ell_3) = \int_0^{\chi_H} \frac{d\chi}{\chi^4} W^3(\chi) B_\delta(\mathbf{k}_1, \mathbf{k}_2, \mathbf{k}_3, a), \quad (21)$$

with $\mathbf{k}_p = \ell_p/\chi$, $p = 1, 2, 3$, for projection of the flat-sky convergence bispectrum B_κ (Schneider et al. 1998; Hu 1999; Takada & Jain 2003a,b, 2004; Dodelson & Zhang 2005). The spherical bispectrum $B_\kappa(\ell_1, \ell_2, \ell_3)$ is related to the flat-sky bispectrum $B_\kappa(\ell_1, \ell_2, \ell_3)$ by (Miralda-Escude 1991; Kaiser 1992)

$$B_\kappa(\ell_1, \ell_2, \ell_3) \simeq \begin{pmatrix} \ell_1 & \ell_2 & \ell_3 \\ 0 & 0 & 0 \end{pmatrix} \sqrt{\frac{\prod_{p=1}^3 (2\ell_p + 1)}{4\pi}} B_\kappa(\ell_1, \ell_2, \ell_3), \quad (22)$$

where

$$\begin{pmatrix} \ell_1 & \ell_2 & \ell_3 \\ 0 & 0 & 0 \end{pmatrix}^2 = \frac{1}{2} \int_{-1}^{+1} dx P_{\ell_1}(x) P_{\ell_2}(x) P_{\ell_3}(x), \quad (23)$$

denotes the Wigner-3j symbol, which results from integrating over three Legendre polynomials $P_\ell(x)$ ($x = \cos \theta$). The Wigner-3j symbol nulls configurations which would violate the triangle inequality, $|\ell_i - \ell_j| \leq \ell_k \leq |\ell_i + \ell_j|$ (Abramowitz & Stegun 1972). The factorials in the Wigner-3j symbol are evaluated using the Stirling approximation for the Γ -function,

$$\Gamma(n+1) = n! \quad \text{with} \quad \Gamma(x) \simeq \sqrt{2\pi} \exp(-x) x^{x-\frac{1}{2}}, \quad (24)$$

for $x \gg 1$ (Abramowitz & Stegun 1972). At this point, it is appropriate to recall two important issues related to the weak shear bispectrum as a line of sight-integrated quantity: The line-of-sight integration causes the non-Gaussianities in the convergence to be weaker than that of the source field, as a consequence of the central limit theorem, because many uncorrelated lensing effects (if the Born approximation is invoked and lens-lens coupling is neglected, see Cooray & Hu 2002; Shapiro & Cooray 2006; Krause & Hirata 2010; Schaefer et al. 2011) add up to the signal (Jeong et al. 2011). Secondly, the evaluation of the wave vector $k = \ell/\chi$ in the source field bispectrum B_δ generates a mixing of scales when the distance χ runs over the integration range such that the observed weak lensing bispectrum is a superposition of density field bispectra of varying scale and fixed projected configuration.

4.3 Properties of the weak lensing bispectrum

Fig. A1 gives a 3-dimensional visual impression of the three different bispectra as observed by weak shear. The weak shear bispectra are given as dimensionless bispectra, by multiplication with the prefactor $(\ell_1 \ell_2 \ell_3)^{4/3} \sim \ell^4$. There are clear differences in the configuration dependence: Local non-Gaussianities provide large amplitudes for squeezed configurations, i.e. in the corners of the domain admissible by the triangle inequality, orthogonal non-Gaussianities are largest for folded configurations and the equilateral bispectra assume large values if the three multipole orders are equal.

Fig. 1 illustrates the contribution $dC_\kappa(\ell)/d\chi$ to the spectrum and the contribution $dB_\kappa(\ell, \ell, \ell)/d\chi$ to the equilateral bispectrum as a function of comoving distance. For the relevant range of multipoles, modes with wave numbers in the range $0.1 \dots 1$ Mpc/h are being probed by weak shear, which are larger than those wave numbers measurable in the primary CMB bispectrum and emphasises

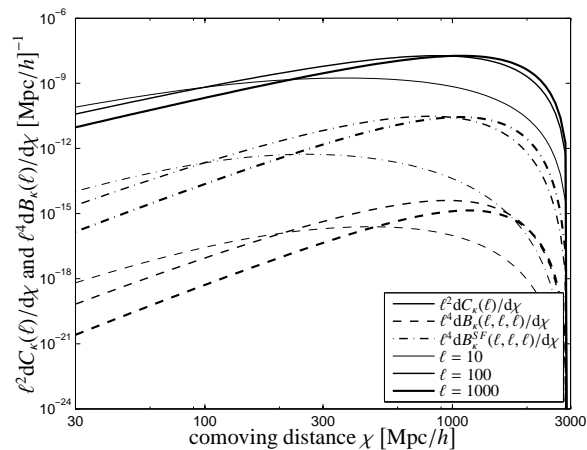


Figure 1. Contributions $\ell^2 dC_\kappa(\ell)/d\chi$ to the lensing spectrum (solid line), and $\ell^4 dB_\kappa(\ell, \ell, \ell)/d\chi$ to the lensing bispectra for both primordial non-Gaussianities (dashed line, $f_{\text{NL}} = 1$) and structure formation non-Gaussianities (dash-dotted line), for $\ell = 10$ (thin lines), $\ell = 100$ (medium lines) and $\ell = 1000$ (thick lines). The bispectra are plotted for the equilateral configuration.

the necessity of measuring f_{NL} in its scale dependence, in a similar way as advocated by Lo Verde et al. (2008) for number counts.

The skewness parameters $S_\kappa(\ell)$ are defined as the ratio between the squared equilateral bispectrum and the cubed spectrum,

$$S_\kappa(\ell) = \sqrt{\frac{B_\kappa^2(\ell, \ell, \ell)}{C_\kappa^3(\ell)}}. \quad (25)$$

$S_\kappa(\ell)$ is proportional to f_{NL} (and to σ_8 to lowest order) and is independent of Ω_m . It will become relevant for the signal-to-noise ratio $\Sigma(\ell)$ (see eqn. 26 in Sect. 5.1). These skewness-parameters are depicted in Fig. 2 as a function of median redshift z_{med} of the lensing survey for both the primordial and the structure formation induced weak lensing bispectrum. The skewness parameters increase with increasing survey depth and in case of primordial non-Gaussianities saturate at redshifts of unity, which is an effect of the time evolution of the gravitational potential being mapped out by weak lensing, as perturbations in the potentials decay in the dark energy-dominated phase and are constant in the matter-dominated phase. Structure formation non-Gaussianities decrease slightly for deeper reaching surveys, which is caused by the fact that the structure formation skewness's are building up during Ω_m -domination, as they scale $\propto D_+/a^3 \sim a$ in contrast to primordial non-Gaussianities in the potential, which are constant with their scaling $\propto (D_+/a)/a^3 \sim \text{const}$. The plot suggests that with the redshift range probed by Euclid the largest-possible skewness's are being observed.

5 STATISTICS

5.1 What signal-to-noise ratio can one expect?

The cumulative signal-to-noise ratio $\Sigma(\ell)$ for the weak lensing bispectrum $B_\kappa(\ell_1, \ell_2, \ell_3)$ up to multipole order ℓ is given by (Hu 1999)

$$\Sigma^2(\ell) = \sum_{\ell_1=\ell_{\text{min}}}^{\ell} \sum_{\ell_2=\ell_{\text{min}}}^{\ell} \sum_{\ell_3=\ell_{\text{min}}}^{\ell} \frac{B_\kappa^2(\ell_1, \ell_2, \ell_3)}{\text{cov}(\ell_1, \ell_2, \ell_3)}. \quad (26)$$

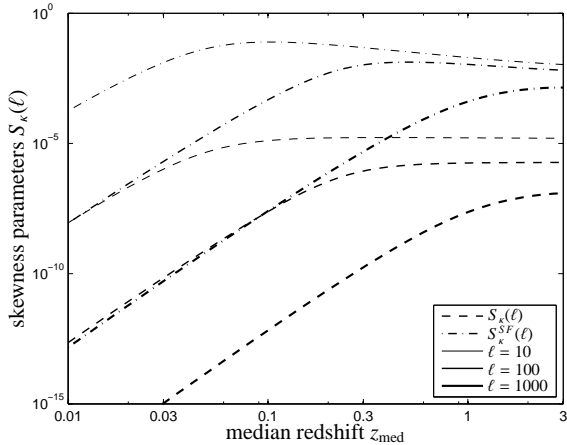


Figure 2. Skewness parameter $S_\kappa(\ell)$ for both primordial non-Gaussianities (dashed line, $f_{\text{NL}} = 1$) and structure formation non-Gaussianities (dash-dotted line) as a function of the survey depth, for $\ell = 10$ (thin lines), $\ell = 100$ (medium lines) and $\ell = 1000$ (thick lines).

The summation is carried out with the condition $\ell_1 \leq \ell_2 \leq \ell_3$ (Takada & Jain 2004), such that the covariance becomes

$$\text{cov}(\ell_1, \ell_2, \ell_3) = \frac{\Delta(\ell_1, \ell_2, \ell_3)}{f_{\text{sky}}} \tilde{C}(\ell_1) \tilde{C}(\ell_2) \tilde{C}(\ell_3), \quad (27)$$

where the function $\Delta(\ell_1, \ell_2, \ell_3)$ counts the multiplicity of triangle configurations and is defined as

$$\Delta(\ell_1, \ell_2, \ell_3) = \begin{cases} 6, & \ell_1 = \ell_2 = \ell_3 \\ 2, & \ell_i = \ell_j \text{ for } i \neq j \\ 1, & \ell_1 \neq \ell_2 \neq \ell_3 \neq \ell_1 \end{cases} \quad (28)$$

f_{sky} denotes the fraction of the observed sky and is set to $f_{\text{sky}} = 1/2$ for Euclid. The observed spectra

$$\tilde{C}(\ell) = C(\ell) + \frac{\sigma_\epsilon^2}{n}, \quad (29)$$

with the number density of ellipticity measurements per steradian n , which is set to 40 galaxies per squared arcminute, corresponding to the projected Euclid performance. Instead of a direct summation over ℓ_1, ℓ_2, ℓ_3 we use a Monte-Carlo integration technique and consider the evaluation of eqn. (26) as a three-dimensional integration, for which we use publicly available CUBA-library (Hahn 2005).

The cumulative signal-to-noise ratio $\Sigma(\ell)$ for a measurement of the weak shear bispectrum is depicted in Fig. 3 as a function of ℓ and for all three non-Gaussianity types. As the signal strength Σ is proportional to the non-Gaussianity parameter f_{NL} , it is convenient to plot the ratio $\Sigma(\ell)/f_{\text{NL}}$. The plot suggests that weak lensing bispectra sourced by primordial non-Gaussianities could only be measured with Euclid for f_{NL} significantly larger than 100. Orthogonal bispectra are weaker by a factor of 3 compared to local bispectra, and equilateral bispectra generate the weakest signal, being a factor of 8 weaker than local non-Gaussianities. The four different MC-integration algorithms agree well in their results for $\Sigma(\ell)$, and when the number of sampling points is chosen to be $\propto \ell$, the algorithms retain accuracies, indicating that the adaptive algorithms take account of the symmetry properties of the integrand. At $\ell = 1000$, it is sufficient to compute $\mathcal{O}(10^5)$ samples, which reduces the number of evaluations of the integrand by a factor of 10^4 compared to the exact evaluation, which would require $\mathcal{O}(10^9)$ evaluations, for

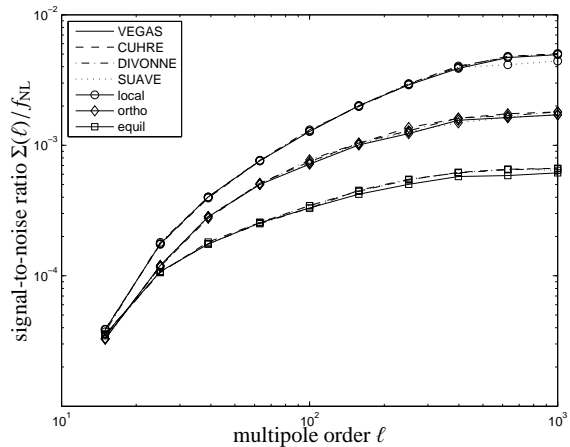


Figure 3. Cumulative signal-to-noise ratio $\Sigma(\ell)/f_{\text{NL}}$ as a function of maximum multipole order ℓ , for local (circles), orthogonal (lozenges) and equilateral (squares) non-Gaussianities. The figure compares the result from different Monte-Carlo integration routines.

precisions on the sub-percent level. We will restrict ℓ -space integrations to multipoles $\lesssim 1000$, because the increase in signal when extending the ℓ -range is marginal for primordial non-Gaussianities and additionally, it helps to avoid scales influenced by baryonic physics and intrinsic alignments (Semboloni et al. 2008, 2011).

The configuration dependence of the contribution to the integrated signal is given in Fig. A1 in the appendix for the three bispectrum types considered here. The panels show the weak shear bispectrum in units of the noise, $B_\kappa(\ell_1, \ell_2, \ell_3) / \sqrt{\text{cov}(\ell_1, \ell_2, \ell_3)}$ as a function of ℓ_1, ℓ_2 and ℓ_3 . While the local non-Gaussianity provides the largest contributions for squeezed configurations, the orthogonal non-Gaussianity shows a much uniform contribution throughout ℓ -space, and the equilateral non-Gaussianity is only providing significant amplitudes for very small values of ℓ . This behavior is reflected in the cumulative signal-to-noise ratio, as shown in Fig. 3. From the signal-to-noise ratios one can already estimate the accuracy for a measurement of f_{NL} . The conditional Cramér-Rao bounds $\sigma_{f_{\text{NL}}} = 1/\sqrt{F_{f_{\text{NL}}f_{\text{NL}}}}$ on the non-Gaussianity parameter (which are at the same time the non-Gaussianities required to generate a signal of unity) are $\sigma_{f_{\text{NL}}} = 200$ (local), $\sigma_{f_{\text{NL}}} = 575$ (orthogonal) and $\sigma_{f_{\text{NL}}} = 1628$ (equilateral) which is significantly weaker than other probes such as the primary CMB, due to the Gaussianising effect of the line-of-sight integrations (Jeong et al. 2011).

5.2 Would one misestimate f_{NL} using the wrong bispectrum?

The χ^2 -functional constructed for measuring the noise-weighted mismatch between the true bispectrum B'_κ and the wrongly assumed bispectrum B_κ^w for interpreting the data reads:

$$\chi^2 = \sum_{\ell_1=\ell_{\min}}^{\ell} \sum_{\ell_2=\ell_{\min}}^{\ell} \sum_{\ell_3=\ell_{\min}}^{\ell} \frac{[\alpha B_\kappa^w(\ell_1, \ell_2, \ell_3) - B'_\kappa(\ell_1, \ell_2, \ell_3)]^2}{\text{cov}(\ell_1, \ell_2, \ell_3)} \quad (30)$$

and yields the best fitting α from the minimisation $\partial\chi^2/\partial\alpha = 0$.

The variable α measures the ratio between the wrongly inferred non-Gaussianity parameter f_{NL} and the true value, and is given by Fig. 4 as a function of maximum multipole order considered in the integration of the χ^2 -functional. For weak signals this ratio is very close to unity, and differences emerge when the

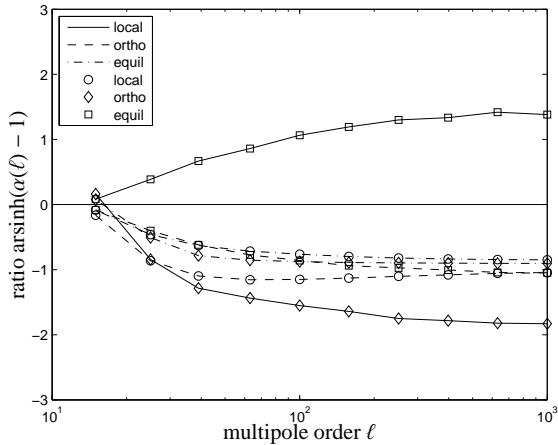


Figure 4. The ratio $\alpha(\ell)$ of inferred f_{NL} -value to the true f_{NL} -value as a function of maximum multipole order ℓ . The true non-Gaussianity model is indicated by the line style, whereas the wrongly chosen non-Gaussianity model is given by the marker style: local (circles, solid lines), orthogonal (lozenges, dashed lines) and equilateral (squares, dash-dotted lines) non-Gaussianities.

integration is carried out to larger multipoles, and the signal becomes stronger. Misestimations in f_{NL} up to half an order of magnitude appear possible, including wrong signs for f_{NL} -estimates. Most combinations of B'_k and B''_k yield very small values for the estimated f_{NL} -parameter (equivalently, $\alpha \simeq -1$) when choosing the wrong non-Gaussianity. Again, the evaluations necessary for determining α are carried out as an MC-integration with the CUBA-library (Hahn 2005).

5.3 Would one notice fitting the wrong bispectrum?

Now, the question appears if one would notice the assumption of a wrong primordial bispectrum when fitting for the non-Gaussianity parameter f_{NL} . This can be quantified by the probability q of obtaining data more extreme than the one at hand. This probability q (Fisher's p -value) is given as a function of the true f_{NL} under the assumption of a Gaussian likelihood, which is well justified given the very large number of degrees of freedom (although doubts have been raised about how accurate this is, see Smith et al. 2011). As shown in Fig. 5 for all combinations between true non-Gaussianity types and wrongly fitted non-Gaussianity models, this probability drops very rapidly towards very small numbers for f_{NL} -values of a few hundred, indicating that it would be very difficult to reconcile non-Gaussianities of that strength with observations if the wrong non-Gaussianity model had been chosen. For f_{NL} -values smaller than 100 the signal is so weak that no significant discrepancies between data and model appear, for any type of non-Gaussianity.

5.4 Do parameter constraints depend on non-Gaussianity?

The Fisher-matrix formalism (Tegmark et al. 1997) is widely used in cosmology for deriving parameter forecasts, and requires in the case of the bispectrum as the signal-to-noise ratio the summation over all triangle configurations:

$$F_{\mu\nu} = \sum_{\ell_1=\ell_{\min}}^{\ell} \sum_{\ell_2=\ell_{\min}}^{\ell} \sum_{\ell_3=\ell_{\min}}^{\ell} \frac{\partial B_k}{\partial x_\mu} \frac{1}{\text{cov}(\ell_1, \ell_2, \ell_3)} \frac{\partial B_k}{\partial x_\nu}. \quad (31)$$

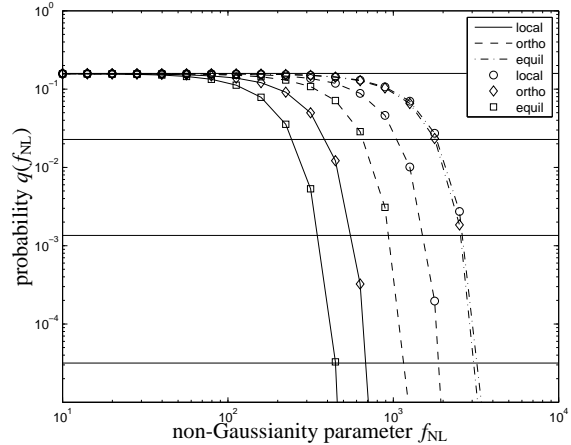


Figure 5. Probability $q(f_{\text{NL}})$ of obtaining data as extreme as a wrong fit to the weak lensing bispectrum by choosing the wrong non-Gaussianity model (indicated by the line style) to data (indicated by the marker style): local (circles, solid lines), orthogonal (lozenges, dashed lines) and equilateral (squares, dash-dotted lines) non-Gaussianities. The horizontal lines indicate 1, 2, 3, 4 σ confidence intervals and ℓ has been set to 1000.

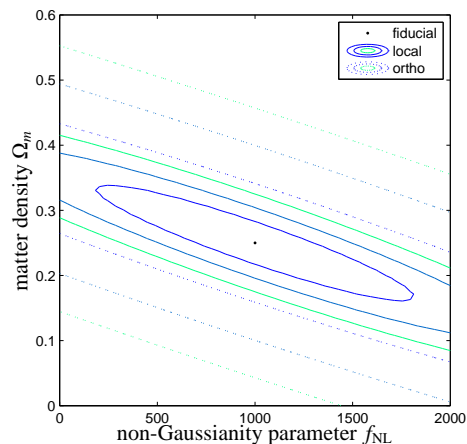


Figure 6. 1 σ , 2 σ and 3 σ -constraints on the non-Gaussianity parameter f_{NL} and the matter density Ω_m , for the local non-Gaussianity (solid lines) and the orthogonal non-Gaussianity (dotted lines) at $\ell = 1000$, from a numerical MC-integration of the Fisher-matrix.

The explicit summation can be replaced by a $d^3\ell$ -integration, which can be carried out using the MC-technique outlined in Sect. 5.1. Resulting simultaneous constraints on Ω_m and f_{NL} from the weak shear bispectrum sourced only by primordial non-Gaussianities with no other priors are given in Fig. 6 for local and orthogonal models at a reference $f_{\text{NL}} = 1000$. The equilateral bispectrum does not constrain the parameter pair in a meaningful way due to the weak signal.

6 SYSTEMATICS DUE TO STRUCTURE FORMATION

6.1 Can one subtract the structure formation bispectrum?

Naturally, the small primordial non-Gaussianities are superseded by much stronger non-Gaussianities due to nonlinearities in the cosmic structure formation processes, which affects the measurability of f_{NL} . There exists an accurate description of the structure formation bispectrum provided by Eulerian perturbation theory on the scales of interest (compare Sect. 3.2, and Bernardeau et al. 2002), if the cosmology is known – but there are always uncertainties in the cosmological parameter set, which would result in an uncertainty in predicting the structure formation bispectrum. If the structure formation bispectrum is not properly subtracted from the observed bispectrum, there will be errors in the estimation of the non-Gaussianity parameter f_{NL} for the primordial bispectrum, which can be quantified with the χ^2 -functional,

$$\chi^2 = \sum_{\ell_1=\ell_{\min}}^{\ell} \sum_{\ell_2=\ell_{\min}}^{\ell} \sum_{\ell_3=\ell_{\min}}^{\ell} \frac{[\alpha B'_k(\ell_1, \ell_2, \ell_3) - \Delta B_k(\ell_1, \ell_2, \ell_3)]^2}{\text{cov}(\ell_1, \ell_2, \ell_3)}, \quad (32)$$

describing the fit of a primordial bispectrum B'_k to data ΔB_k ,

$$\Delta B_k(\ell_1, \ell_2, \ell_3) = B'_k(\ell_1, \ell_2, \ell_3) + B_k^{\text{SF}}(\ell_1, \ell_2, \ell_3) - B_k^{\text{w,SF}}(\ell_1, \ell_2, \ell_3) \quad (33)$$

which contain the true primordial bispectrum B'_k itself, the very large structure formation bispectrum B^{SF} for the true cosmology, from which the structure formation bispectrum $B^{\text{w,SF}}$ has been subtracted, possibly incompletely, by assuming the wrong cosmology. Derivation $\partial\chi^2/\partial\alpha = 0$ yields the best fitting α , which is related to the misestimated $f_{\text{NL}}^{\text{w}} = \alpha f_{\text{NL}}$ and the deviation from the true non-Gaussianity $\delta = \alpha - 1$.

Distributions $p(\delta)d\delta$ have been derived for all bispectrum types by drawing 10^3 samples from a Gaussian likelihood for the parameters Ω_m , σ_8 , h , n_s and w of a standard spatially flat dark energy model. The covariance matrix has been constructed using the icosmo resource for the Euclid weak lensing and BAO data (Refregier et al. 2011), and provides an excellent prior on the cosmological parameters. By this sampling process of δ it is possible to propagate the entire uncertainty in the cosmological parameter set onto the estimate of f_{NL} . As shown by Fig. 7, the resulting distribution is very close to Gaussian, with zero mean and standard deviations of $\sigma_{f_{\text{NL}}} = 119$ (local), $\sigma_{f_{\text{NL}}} = 372$ (orthogonal) and $\sigma_{f_{\text{NL}}} = 511$ (equilateral), which is similar to the statistical uncertainty of measuring f_{NL} and thus constitutes a serious error. The width of the distributions are independent of the true value f_{NL} , and the relative error δ/f_{NL} scales $\propto 1/f_{\text{NL}}$. Misestimates of that magnitude make it very difficult to assign a primordial origin to a non-zero residual bispectrum, given the current bounds on f_{NL} . All integrations were computed up to $\ell = 1000$.

6.2 What happens if a better prior is available?

The uncertainty in predicting the weak shear bispectrum generated by nonlinear structure formation can be reduced if a stronger prior on the cosmological parameter set is available or if the complexity of the model is reduced, e.g. if the w CDM dark energy cosmology would be replaced by the simpler Λ CDM cosmology. Fig. 8 illustrates the distributions $p(\delta)d\delta$ of the difference δ between the inferred non-Gaussianity parameter and the true parameter, if the contamination of the bispectrum is computed by drawing 10^3 sample w CDM cosmologies from a Gaussian likelihood whose covariance matrix incorporates constraints from Euclid weak shear spectra, Euclid baryon acoustic oscillations and in addition Planck's

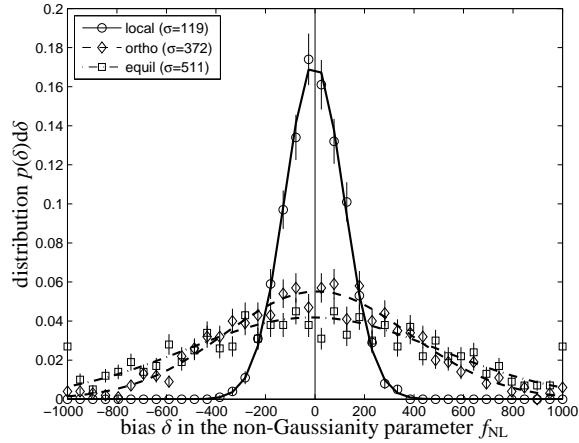


Figure 7. Distributions $p(\delta)d\delta$ of the bias δ between the inferred non-Gaussianity parameter and the true parameter f_{NL} if the structure formation bispectrum is not completely removed, due to uncertainties in the cosmological model, for local (circles, solid line), orthogonal (lozenges, dashed line) and equilateral (squares, dash-dotted line) non-Gaussianities. As priors, Euclid weak lensing and baryon acoustic oscillations were used.

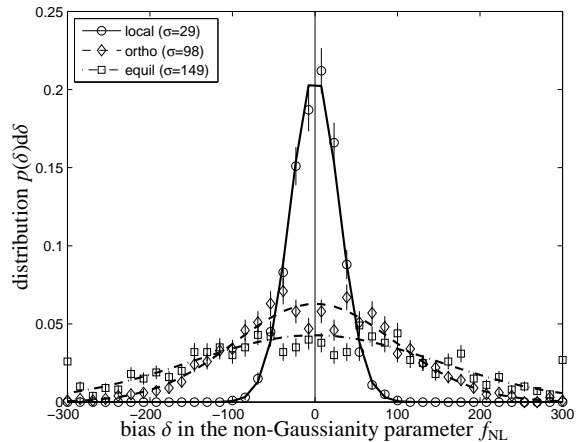


Figure 8. Distributions $p(\delta)d\delta$ of the bias δ with an enhanced prior for the cosmological model with constraints from weak lensing, baryon acoustic oscillations (both Euclid) and CMB temperature and polarisation spectra (Planck), for local (circles, solid line), orthogonal (lozenges, dashed line) and equilateral (squares, dash-dotted line) non-Gaussianities.

constraints from the observation of primary CMB temperature and polarisation spectra. In comparison to the distributions shown in Fig. 7, the width is now much reduced, by about a factor of 4, allowing measurements down to smaller values for f_{NL} . The specific uncertainties are $\sigma_{f_{\text{NL}}} = 29$ (local), $\sigma_{f_{\text{NL}}} = 98$ (orthogonal) and $\sigma_{f_{\text{NL}}} = 149$ (equilateral), all stated as standard deviations of the distribution $p(\delta)d\delta$. These uncertainties are below current bounds on f_{NL} and are small enough for studies of primordial non-Gaussianities. Again, all integrations were carried out up to $\ell = 1000$.

7 SUMMARY

The topic of this paper are measurements of primordial bispectra in weak shear data from Euclid, comparisons between different types of non-Gaussianity configuration dependences, statistical questions concerning the inference of the non-Gaussianity parameter f_{NL} and the removal of the much stronger structure formation induced bispectrum. Although not as sensitive as observations of the CMB-bispectrum or the galaxy bispectrum for scale-free non-Gaussianities, weak lensing can place useful independent constraints on non-Gaussianities, in particular on smaller scales where CMB bounds might not apply. It is less prone to systematics than other large-scale structure probes and provides a direct linear mapping of the density field, which conserves its statistical properties.

(i) Primordial non-Gaussianities provide a rather weak signal in the weak shear bispectrum (because of the Gaussianising effect of the line-of-sight integration, see Jeong et al. 2011), and signal-to-noise ratios of order unity can only be expected for $f_{\text{NL}} = 200, 575, 1628$ for local, orthogonal and equilateral non-Gaussianities, respectively, where this measurement is most sensitive to scales $0.1 \dots 1 \text{ (Mpc}/h)^{-1}$. These bounds are weaker than those from e.g. observations of the CMB bispectrum, but will serve nevertheless for cross validation, in particular given the absence of strong systematics in weak shear data, or as bounds on scale-dependent non-Gaussianity, because weak lensing maps out scales which are not constrained by the CMB and is sensitive to scales probed by number counts.

(ii) Configuration space integrations can be very efficiently carried out by Monte-Carlo integration schemes, at a fraction of the computational cost. Computations of the signal-to-noise ratio, of χ^2 -functionals or of the Fisher-matrix $F_{\mu\nu}$ can be done with accuracies below a percent with $O(10^5)$ evaluations instead of $O(10^9)$ evaluations for the direct sum over ℓ_1, ℓ_2 and ℓ_3 . Very good results were obtained with the CUBA library (Hahn 2005).

(iii) Fitting the wrong bispectrum type to data yields serious misestimates in the non-Gaussianity parameter f_{NL} . Depending on the combination of true and false model there are two cases: either the estimated f_{NL} becomes very small, or the estimate for f_{NL} is a factor of $\sim \pm 3$ too large. When looking at numerical values for the χ^2 -functional, one would notice strong discrepancies between data and model when fitting the wrong non-Gaussianity type from values of f_{NL} of a few hundred on.

(iv) The much stronger structure formation bispectrum can be subtracted with a prediction of its bispectrum from perturbation theory if the cosmology is known precisely enough. Propagating the uncertainty in the cosmological parameter set onto the misestimation of f_{NL} if the structure formation bispectrum is not correctly subtracted yielded typical uncertainties of 29, 98 and 149 for local, orthogonal and equilateral non-Gaussianities, much less than the statistical accuracy. As a prior on the cosmological parameters we assumed a Gaussian likelihood for a Λ CDM model combining Euclid's weak shear with baryon acoustic oscillations and Planck's observations of primary CMB anisotropies. Similar ratios between the numerical value of f_{NL} and the standard cosmological parameters were found by Pace et al. (2011).

Many of our investigations can be straightforwardly generalised to other probes of large-scale structure statistics. We intend to generalise our investigations to higher polyspectra and to apply ideas from Bayesian model selection (Trotta 2007, 2008) for assigning probabilities to the problem of choosing the correct non-Gaussianity type.

ACKNOWLEDGEMENTS

We acknowledge the use of the formidable icosmo resource for computing a joint Fisher matrix for baryon acoustic oscillations and the weak shear spectrum. We would like to thank Maik Weber and Youness Ayaita for providing a CMB Fisher matrix for the Planck survey characteristics, Matthias Bartelmann for his suggestions, Patricio Vielva for his help in clarifying statistical questions and Tommaso Giannantonio for thoughtful comments on our draft. Our work was supported by the German Research Foundation (DFG) within the framework of the excellence initiative through the Heidelberg Graduate School of Fundamental Physics and by the German National Academic Foundation. This paper is listed as preprint BI-TP 2011/20.

REFERENCES

- Abramowitz M., Stegun I. A., 1972, Handbook of Mathematical Functions. Handbook of Mathematical Functions, New York: Dover, 1972
- Alabidi L., Malik K., Byrnes C. T., Choi K.-Y., 2010, JCAP, 1011, 037
- Alishahiha M., Silverstein E., Tong D., 2004, Phys.Rev., D70, 123505
- Arkani-Hamed N., Creminelli P., Mukohyama S., Zaldarriaga M., 2004, JCAP, 0404, 001
- Arroja F., Enea Romano A., Sasaki M., 2011, ArXiv e-prints 1106.5384
- Bardeen J. M., 1980, Phys.Rev., D22, 1882
- Bardeen J. M., Bond J. R., Kaiser N., Szalay A. S., 1986, ApJ, 304, 15
- Bardeen J. M., Steinhardt P. J., Turner M. S., 1983, Phys.Rev., D28, 679
- Barnaby N., 2010, Adv.Astron., 2010, 156180
- Barnaby N., Cline J. M., 2008, JCAP, 0806, 030
- Bartelmann M., 2010, Classical and Quantum Gravity, 27, 233001
- Bartelmann M., Schneider P., 2001, Physics Reports, 340, 291
- Bartolo N., Fasiello M., Matarrese S., Riotto A., 2010, JCAP, 1012, 026
- Bartolo N., Komatsu E., Matarrese S., Riotto A., 2004, Physics Reports, 402, 103
- Battefeld D., Battefeld T., Byrnes C., Langlois D., 2011, arXiv 1106.1891
- Becker A., Huterer D., Kadota K., 2011, JCAP, 1101, 006
- Bernardeau F., Colombi S., Gaztañaga E., Scoccimarro R., 2002, Physics Reports, 367, 1
- Bernardeau F., Uzan J.-P., 2003, Phys. Rev. D, 67, 121301
- Bernardeau F., van Waerbeke L., Mellier Y., 2003, A&A, 397, 405
- Burrage C., Ribeiro R. H., Seery D., 2011, arXiv 1103.4126
- Byrnes C. T., Choi K.-Y., Hall L. M., 2008, JCAP, 0810, 008
- Byrnes C. T., Enqvist K., Takahashi T., 2010, JCAP, 1009, 026
- Byrnes C. T., Gerstenlauer M., Nurmi S., Tasinato G., Wands D., 2010, JCAP, 10, 4
- Cabella P., Liguori M., Hansen F. K., Marinucci D., Matarrese S., Moscardini L., Vittorio N., 2005, MNRAS, 358, 684
- Casaponsa B., Barreiro R. B., Curto A., Martínez-González E., Vielva P., 2011, MNRAS, 411, 2019
- Chen X., 2005, Phys.Rev., D72, 123518
- Chen X., 2011, arXiv 1104.1323
- Chen X., Easther R., Lim E. A., 2007, JCAP, 0706, 023
- Chen X., Easther R., Lim E. A., 2008, JCAP, 0804, 010

- Chen X., Huang M.-x., Kachru S., Shiu G., 2007, JCAP, 0701, 002
- Cheung C., Creminelli P., Fitzpatrick A., Kaplan J., Senatore L., 2008, JHEP, 0803, 014
- Cooray A., Hu W., 2002, ApJ, 574, 19
- Creminelli P., Nicolis A., Senatore L., Tegmark M., Zaldarriaga M., 2006, JCAP, 5, 4
- Curto A., Martínez-González E., Barreiro R. B., 2009, ApJ, 706, 399
- Desjacques V., Seljak U., 2010a, Classical and Quantum Gravity, 27, 124011
- Desjacques V., Seljak U., 2010b, Advances in Astronomy, 2010
- Dodelson S., Zhang P., 2005, Phys. Rev. D, 72, 083001
- Dvali G., Gruzinov A., Zaldarriaga M., 2004, Phys.Rev., D69, 023505
- Elliston J., Mulryne D. J., Seery D., Tavakol R., 2011, arXiv 1106.2153
- Fedeli C., Carbone C., Moscardini L., Cimatti A., 2011, MNRAS, 414, 1545
- Fedeli C., Pace F., Moscardini L., Grossi M., Dolag K., 2011, ArXiv e-prints 1103.5396
- Fergusson J., Shellard E., 2009, Phys.Rev., D80, 043510
- Fergusson J. R., Liguori M., Shellard E. P. S., 2010, Phys. Rev. D, 82, 023502
- Fergusson J. R., Shellard E. P. S., 2007, Phys. Rev. D, 76, 083523
- Fry J. N., 1984a, ApJL, 277, L5
- Fry J. N., 1984b, ApJ, 279, 499
- Gott J. R., Colley W. N., Park C.-G., Park C., Mugnolo C., 2007, MNRAS, 377, 1668
- Hahn T., 2005, Computer Physics Communications, 168, 78
- Hikage C., Matsubara T., Coles P., Liguori M., Hansen F. K., Matarrese S., 2008, MNRAS, 389, 1439
- Hu W., 1999, ApJL, 522, L21
- Huang Q.-G., 2010, JCAP, 1011, 026
- Jeong D., Schmidt F., Sefusatti E., 2011, ArXiv e-prints 1104.0926
- Kaiser N., 1992, ApJ, 388, 272
- Komatsu E., 2003, New Astronomy, 47, 797
- Komatsu E., 2010, Class.Quant.Grav., 27, 124010
- Komatsu E., Afshordi N., Bartolo N., Baumann D., Bond J., et al., 2009, arXiv 0902.4759
- Komatsu E., Dunkley J., Nolte M. R., Bennett C. L., Gold B., Hinshaw G., Jarosik N., Larson D., Limon M., Page L., Spergel D. N., Halpern M., Hill R. S., Kogut A., Meyer S. S., Tucker G. S., Weiland J. L., Wollack E., Wright E. L., 2009, ApJS, 180, 330
- Komatsu E., Smith K. M., Dunkley J., et al. 2011, ApJS, 192, 18
- Krause E., Hirata C. M., 2010, A&A, 523, A28+
- Langlois D., 2011, ArXiv e-prints 1102.5052
- Lehners J.-L., 2010, Adv.Astron., 2010, 903907
- Li M., Wang T., Wang Y., 2008, JCAP, 0803, 028
- Limber D. N., 1954, ApJ, 119, 655
- Linder E. V., Jenkins A., 2003, MNRAS, 346, 573
- Lo Verde M., Miller A., Shandera S., Verde L., 2008, JCAP, 4, 14
- Lyth D. H., Ungarelli C., Wands D., 2003, Phys.Rev., D67, 023503
- Marian L., Hilbert S., Smith R. E., Schneider P., Desjacques V., 2011, ApJL, 728, L13+
- Matsubara T., 2011, Phys. Rev. D, 83, 083518
- Ménard B., Bartelmann M., Mellier Y., 2003, A&A, 409, 411
- Miralda-Escude J., 1991, ApJ, 380, 1
- Mukherjee P., Wang Y., 2004, ApJ, 613, 51
- Munshi D., van Waerbeke L., Smidt J., Coles P., 2011, ArXiv e-prints
- Noller J., Magueijo J., 2011, Phys.Rev., D83, 103511
- Pace F., Moscardini L., Bartelmann M., Branchini E., Dolag K., Grossi M., Matarrese S., 2011, MNRAS, 411, 595
- Refregier A., Amara A., Kitching T. D., Rassat A., 2011, A&A, 528, A33+
- Riotto A., 2002, hep-ph/0210162, pp 317–413
- Riotto A., Sloth M. S., 2011, Phys.Rev., D83, 041301
- Sachs R., Wolfe A., 1967, Astrophys.J., 147, 73
- Sahni V., Coles P., 1995, Physics Reports, 262, 1
- Schaefer B. M., Heisenberg L., Fotios Kalovidouris A., Bacon D. J., 2011, ArXiv e-prints 1101.4769
- Schneider P., van Waerbeke L., Jain B., Kruse G., 1998, MNRAS, 296, 873
- Scoccimarro R., Couchman H. M. P., 2001, MNRAS, 325, 1312
- Seery D., Lidsey J. E., 2005, JCAP, 0506, 003
- Sefusatti E., Liguori M., Yadav A. P., Jackson M. G., Pajer E., 2009, JCAP, 0912, 022
- Semboloni E., Heymans C., van Waerbeke L., Schneider P., 2008, MNRAS, 388, 991
- Semboloni E., Hoekstra H., Schaye J., van Daalen M. P., McCarthy I. G., 2011, ArXiv e-prints 1105.1075
- Semboloni E., Schrabback T., van Waerbeke L., Vafaei S., Hartlap J., Hilbert S., 2011, MNRAS, 410, 143
- Senatore L., Smith K. M., Zaldarriaga M., 2010, JCAP, 1001, 028
- Shandera S., Dalal N., Huterer D., 2011, JCAP, 1103, 017
- Shapiro C., Cooray A., 2006, Journal of Cosmology and Astro-Particle Physics, 3, 7
- Shi X., Schneider P., Joachimi B., 2011, ArXiv e-prints
- Silverstein E., Tong D., 2004, Phys.Rev., D70, 103505
- Smith T. L., Kamionkowski M., Wandelt B. D., 2011, ArXiv e-prints
- Sugiyama N., 1995, ApJS, 100, 281
- Takada M., Jain B., 2003a, MNRAS, 340, 580
- Takada M., Jain B., 2003b, MNRAS, 344, 857
- Takada M., Jain B., 2004, MNRAS, 348, 897
- Tegmark M., Taylor A. N., Heavens A. F., 1997, ApJ, 480, 22
- Trotta R., 2007, MNRAS, 378, 72
- Trotta R., 2008, Contemporary Physics, 49, 71
- Turner M. S., White M., 1997, Phys. Rev. D, 56, 4439
- Verde L., 2010, Advances in Astronomy, 2010
- Vielva P., Sanz J. L., 2009, MNRAS, 397, 837
- Vielva P., Sanz J. L., 2010, MNRAS, 404, 895
- Wang L., Steinhardt P. J., 1998, ApJ, 508, 483
- Yadav A. P. S., Wandelt B. D., 2008, Physical Review Letters, 100, 181301

APPENDIX A: CONFIGURATION DEPENDENCE

Fig. A1 compares the configuration dependence of the bispectrum and of the signal strength in a weak lensing experiment. As a representation, we chose to plot the dimensionless weak convergence bispectrum $(\ell_1 \ell_2 \ell_3)^{4/3} B_\kappa(\ell_1, \ell_2, \ell_3)$ and the convergence bispectrum in units of the noise, $B_\kappa(\ell_1, \ell_2, \ell_3) / \sqrt{\text{cov}(\ell_1, \ell_2, \ell_3)}$, which when added in quadrature yields the signal-to-noise ratio. The factor $(\ell_1 \ell_2 \ell_3)^{4/3} \sim \ell^4$ makes the angular bispectra dimensionless.

This paper has been typeset from a $\text{\TeX}/\text{\LaTeX}$ file prepared by the author.

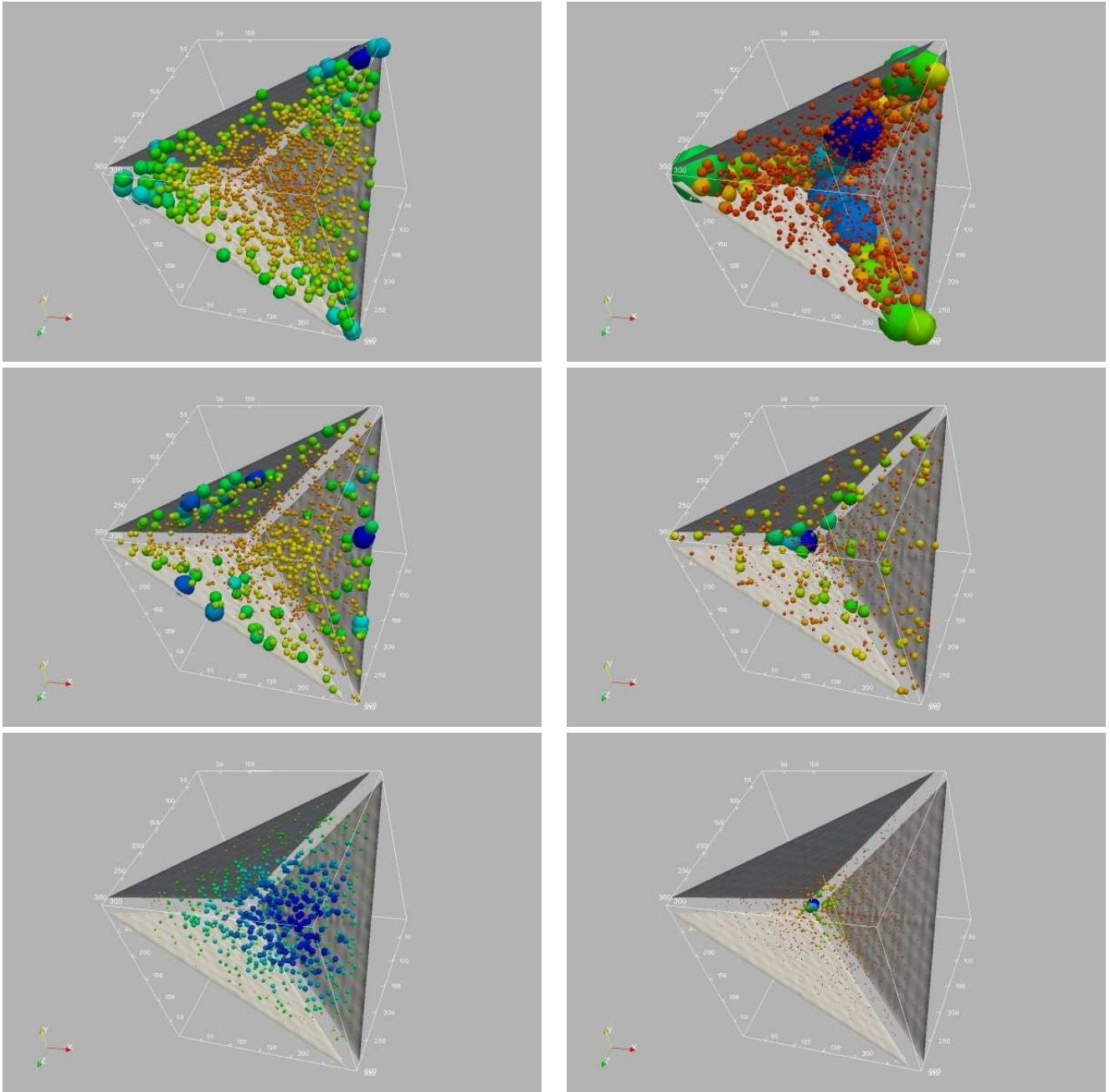


Figure A1. Configuration dependence $(\ell_1 \ell_2 \ell_3)^{4/3} B_{\kappa}(\ell_1, \ell_2, \ell_3)$ (first column) and signal-to-noise ratio $B_{\kappa}(\ell_1, \ell_2, \ell_3) / \sqrt{\text{cov}(\ell_1, \ell_2, \ell_3)}$ (second column) of the weak lensing bispectrum, for local (first row), orthogonal (second row) and equilateral (third row) non-Gaussianities. The size of the blobs and their colour is proportional to the bispectrum, where a correct relative normalisation in the columns is maintained. Configurations outside the grey bounding planes violate the triangle inequality.